Improving light efficiency in multispectral imaging via complementary notch filters

Theresa Panther*, Maximilian Schambach*, and Michael Heizmann

Karlsruhe Institute of Technology, Institute of Industrial Information Technology,
Hertzstr. 16, 76187 Karlsruhe, Germany

ABSTRACT

We propose a novel multispectral imaging technique employing complementary notch filters instead of bandpass filters which are conventionally used in filter-based multispectral cameras. Therefore, only little power of the incoming photon signal is lost and thus the SNR of the multispectral data can be significantly improved. To validate the proposed approach, simulations of conventional bandpass filters as well as complementary notch filters are presented. To compare the resulting SNRs, the EMVA 1288 standard is adopted in such a way that it is applicable to notch filter-based multispectral cameras. It is found that the SNR can be significantly improved by using complementary filters instead of the conventional bandpass filters, especially at high spectral resolution.

Keywords: multispectral imaging, complementary filters, EMVA 1288

1. INTRODUCTION

Digital cameras most prevalent in consumer electronics are color cameras which capture a 3-channel RGB color image. In many scientific or industrial applications however, color images are not sufficient and cameras that are able to sample the electromagnetic spectrum more densely are required. To this end, multi- or hyperspectral cameras, i.e., cameras that capture a spatially resolved spectrum of a scene, have been developed. These spectral cameras have found applications in remote sensing,[1] farming and agriculture,[2,3] material abundance estimation,[4] sorting tasks,[5,6] medical diagnostics,[7] food inspection,[8] and more.

There are mainly two categories of spectral cameras: dispersion-based and filter-based cameras. Dispersion-based cameras use prisms or gratings to code the spectral dependence of the incoming spectrum in the spatial domain. The most commonly used dispersion-based cameras are hyperspectral line-scan cameras as well as recent snapshot designs such as the Coded Aperture Snapshot Spectral Imagers (CASSI) and its derivatives.[9,10,11] While dispersion-based cameras offer a very high spectral resolution, their optical design is often complex, bulky and challenging to calibrate mechanically. Filter-based cameras on the other hand employ spectral filters to spectrally sample a scene. The spectral filters can either be used to perform several measurements each with a different filter (spectral scanning) or used as a pixel-wise spectral mask similar to the most commonly used techniques in color imaging based on Bayer-pattern sensors. Filter-based cameras are usually more compact and robust compared to diffraction-based ones. Furthermore, spectrally masked sensors can be manufactured using existing, well scaling technology[12,13] opening spectral imaging to the mass market. Compared to diffraction-based spectral imaging techniques however, conventional filter-based spectral cameras have the major disadvantage that only a small fraction of the incident light's power is transmitted by the filters and ultimately captured by the sensor. The higher the spectral resolution of the camera, the narrower the individual filters and the fewer photons can be detected per wavelength range. At very high resolution, heavily cooled electron multiplying CCD sensonrs are used in combination with very narrow bandpass filters, usually acousto-optic tunable filters. This tradeoff is a significant limitation of bandpass filter-based spectral cameras.

To overcome this dilemma, we propose to use notch filters in multispectral imaging. We will formulate this complementary sampling technique rigorously in Section 2. By transmitting a large amount of the incoming spectral power, the usage of notch filters results in a much higher signal-to-noise ratio (SNR) of the captured

---

Further author information: {firstname.lastname}@kit.edu
*Equal contribution.

multispectral data which we will show in detail in Section 3 and 4. While complementary sampling approaches have been investigated in color imaging, sampling the complementary colors cyan, magenta, and yellow instead of red, green, and blue[14, 15] the filter width in both cases is very large as compared to those in multi- or hyperspectral imaging. Therefore, the advantages of complementary sampling are not as severe in color imaging as compared to spectral imaging. In the case of multispectral imaging, complementary sampling has drawn only little attention, lacking a detailed sampling formulation and theoretical considerations as well as thorough evaluation.[16]

2. MULTISPECTRAL IMAGING

We consider a multispectral sensor which spectrally samples an incident spectral flux $\Phi(\lambda)$. The sensor has a wavelength dependent sensitivity which is called the quantum efficiency $\eta(\lambda)$. The wavelength range of interest is denoted by $\Lambda = [\Lambda_0, \Lambda_1]$ and limited by the support of the quantum efficiency. For example, silicon-based sensors have a range of $\Lambda_{\mathrm{Si}} = [300\,\mathrm{nm}, 1100\,\mathrm{nm}]$.[17] If one is interested in a smaller wavelength range, for example the visible range $\Lambda_{\mathrm{VIS}} = [450\,\mathrm{nm}, 700\,\mathrm{nm}]$, one can use a bandpass filter or a set of short- and longpass filters to restrict the support of the incident spectral flux.

2.1 Conventional Sampling

The spectral sampling of the spectral flux $\Phi(\lambda)$ over the wavelength range Λ is realized in conventional filter-based multispectral cameras via a set of N bandpass filters with transmission coefficients $\varphi_i(\lambda) : \Lambda \to [0,1]$ centered around the central wavelengths λ_i which are spread out equidistantly across the wavelength range Λ. As an example, we will consider two bandpass filter types. On the one hand, ideal rectangular filters of width $b = (\Lambda_1 - \Lambda_0)/N$ with central wavelengths

$$\lambda_i = \Lambda_0 + ib \tag{1}$$

and transmission coefficients

$$\varphi_i(\lambda) = \begin{cases} 1 & \text{if } |\lambda - \lambda_i| < b/2 \\ 0 & \text{else} \end{cases}, \quad i = 1, 2, \ldots, N. \tag{2}$$

In practise, close-to-ideal bandpass filters can be achieved by high-OD interference filters. And on the other hand, we investigate Gaussian bandpass filters with the same central wavelengths as in the ideal filter case but with Gaussian-like transmission coefficients

$$\varphi_i(\lambda) = \exp\left(-\frac{(\lambda - \lambda_i)^2}{2\sigma^2}\right), \quad i = 1, 2, \ldots N. \tag{3}$$

Here, the standard deviation σ is assumed to be constant across all N bandpass filters and can equivalently be expressed via the full width at half maximum $\mathrm{FWHM} = 2\sqrt{2\ln 2}\,\sigma$. In practise, Fabry-Perot interference filters show a Gaussian-shaped transmission coefficient.

Given the transmission coefficients $\varphi_i(\lambda)$ of the filters and the quantum efficiency $\eta(\lambda)$ of the sensor, the transmitted spectral power c_i of the spectral channel i is calculated as

$$c_i = \int_\Lambda \varphi_i(\lambda)\eta(\lambda)\Phi(\lambda)\,\mathrm{d}\lambda. \tag{4}$$

For example, in the case of the ideal rectangular filters, this simplifies to

$$c_i = \int_{\lambda_i - b/2}^{\lambda_i + b/2} \eta(\lambda)\Phi(\lambda)\,\mathrm{d}\lambda. \tag{5}$$

The total signal power P across the considered wavelength range is given by

$$P = \int_\Lambda \eta(\lambda)\Phi(\lambda)\,\mathrm{d}\lambda. \tag{6}$$

(a) Conventional sampling.
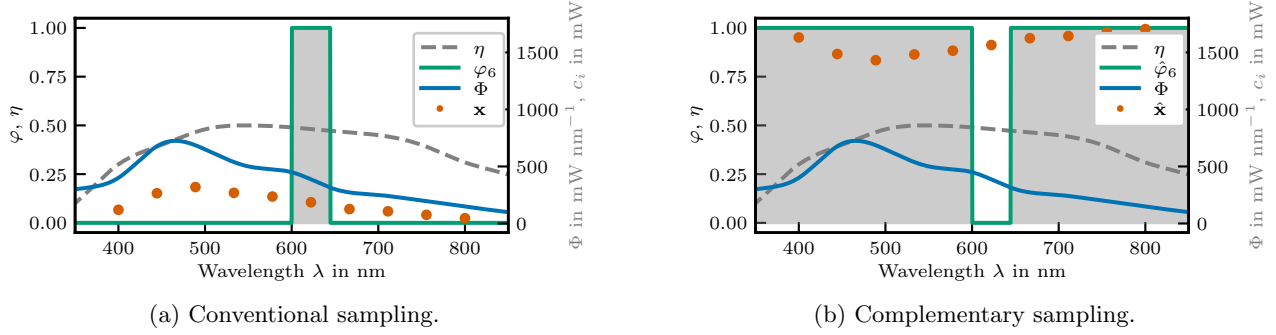
(b) Complementary sampling.

Figure 1: Schematic comparison of conventional (a) and complementary sampling (b) of an arbitrary example spectral flux Φ and quantum efficiency η in the case of $N = 10$ spectral filters. For clarity, only the transmission coefficient of a single filter is shown in each case. The shaded area indicates the sampling range of the corresponding filter.

In this definition, P is the power of $\eta(\lambda)\Phi(\lambda)$ rather than the actual spectral flux $\Phi(\lambda)$. However, this can easily be normalized via calibration (white balance). Finally, we can concatenate the spectral measurements c_i to the vector $\mathbf{x}$ with respect to the standard basis $\mathbf{e}_i$,

$$\mathbf{x} = \sum_{i=1}^{N} c_i \mathbf{e}_i \,. \tag{7}$$

Using narrow bandpass filters in a multispectral camera, high spectral resolution can be achieved. However, narrow bandpass filters lead to a low number of detected photons per spectral channel and therefore to a low power c_i which is depicted in Figure 1. The low power in turn results in a low SNR of the measured data as we will discuss in more detail in Section 3.

2.2 Complementary Sampling

To increase the transmitted power per spectral channel, we propose a multispectral imaging approach using complementary notch filters. Instead of using a collection of N bandpass filters with transmission coefficients $\varphi_i(\lambda)$, we propose to use the complementary filters with transmission coefficient

$$\hat{\varphi}_i(\lambda) = 1 - \varphi_i(\lambda) \tag{8}$$

to sample the spectral flux $\Phi(\lambda)$. The motivation for this is simple: By using notch filters, a large amount of the incident spectral power is transmitted and detected by the sensor resulting in a much larger SNR as compared to the conventional sampling using bandpass filters. At the same time, the set of the used complementary filters result in a multiplexing scheme which provides the same spectral information as the conventional approach as we will discuss shortly.

In complete analogy to the bandpass filter case, we calculate the transmitted spectral power in the case of the complementary filters to

$$\hat{c}_i = \int_\Lambda \hat{\varphi}_i(\lambda)\eta(\lambda)\Phi(\lambda)\,\mathrm{d}\lambda \tag{9}$$

$$= \int_\Lambda \big(1 - \varphi_i(\lambda)\big)\eta(\lambda)\Phi(\lambda)\,\mathrm{d}\lambda = P - c_i \,, \tag{10}$$

where we have used (4) and (6). In a vectorized fashion, analogous to (7), we identify

$$\hat{\mathbf{x}} = P - \mathbf{x} \,. \tag{11}$$

That is, the complementary spectral measurement $\hat{\mathbf{x}}$ is equivalent to the conventional spectral measurement $\mathbf{x}$ if the power P is known. The most straightforward way to obtain P is to perform an additional measurement

without any spectral filters. In fact, measurements without spectral filters in combination with bandpass filters measurements have been studied in the case of color filter array-based cameras.[14] Note that in this case we have not made any use of the explicit definition of the transmission coefficient φ_i. That is, the above equivalence between the spectral measurements with the filters φ_i and the complementary measurements holds for all filters φ_i and is not specific to bandpass filters. While of course bandpass filters are the most commonly used ones in multispectral imaging, this general complementary imaging approach therefore also holds for alternative filters such as short- and longpass filters.

Using bandpass respectively notch filters however makes it possible to calculate the power P from the filtered measurements directly. To this end, the set of filters $\{\varphi_i\}_{i=1}^N$ has to fulfil the sum-to-one constraint

$$\sigma(\lambda) := \sum_i \varphi_i(\lambda) = 1 \tag{12}$$

which can equivalently be expressed using the complementary filters as

$$\frac{\sum_i \hat{\varphi}_i(\lambda)}{N-1} = 1 \,. \tag{13}$$

If the constraint is fulfilled, we can calculate, using (4) and (6),

$$\|\mathbf{x}\|_0 = \sum_i c_i = \int_\Lambda \underbrace{\sum_i \varphi_i(\lambda)}_{=1} \eta(\lambda)\Phi(\lambda)\,\mathrm{d}\lambda = P \tag{14}$$

and analogously

$$\|\hat{\mathbf{x}}\|_1 = (N-1)\int_\Lambda \underbrace{\frac{\sum_i \hat{\varphi}_i(\lambda)}{N-1}}_{=1} \eta(\lambda)\Phi(\lambda)\,\mathrm{d}\lambda = (N-1)P \,. \tag{15}$$

Finally, we obtain from (11)

$$\mathbf{x} = \frac{\|\hat{\mathbf{x}}\|_1}{N-1} - \hat{\mathbf{x}}, \quad \text{or equivalantly} \quad \hat{\mathbf{x}} = \|\mathbf{x}\|_1 - \mathbf{x} \,. \tag{16}$$

That is, if the sum-to-one constraint is fulfilled, the conventional measurement $\mathbf{x}$ and the proposed complementary measurement $\hat{\mathbf{x}}$ are fully equivalent, without the need to measure the total power P separately. In particular, given the complementary measurement $\hat{\mathbf{x}}$, the conventional measurement $\mathbf{x}$ can be calculated from it.

Note that the sum-to-one constraint (12) is exactly fulfilled for the ideal bandpass respectively notch filters as defined in (2). Here, the above result reflects the fact that each wavelength subband which is sampled just once in the case of the conventional bandpass filters is instead sampled $N-1$ times by the complementary filters due to the large filter overlap. Therefore, only little power of the incoming photon signal is lost even at high spectral resolution and the transmitted power $\hat{c}_i$ increases compared to c_i as shown in Figure 1. To be precise, the measured complementary signal $\hat{\mathbf{x}}$ is $(N-1)$-times stronger than the conventionally sampled spectrum $\mathbf{x}$, since from (14) and (15) it follows

$$\|\hat{\mathbf{x}}\|_1 = (N-1)\|\mathbf{x}\|_1 \,. \tag{17}$$

In those instances where the constraint (12) is not fulfilled exactly, which is the case for the considered Gaussian bandpass and notch filters, equations (14)–(16) only hold approximately. We investigate the sum-to-one constraint in the case of Gaussian filters in more detail in Section 4.
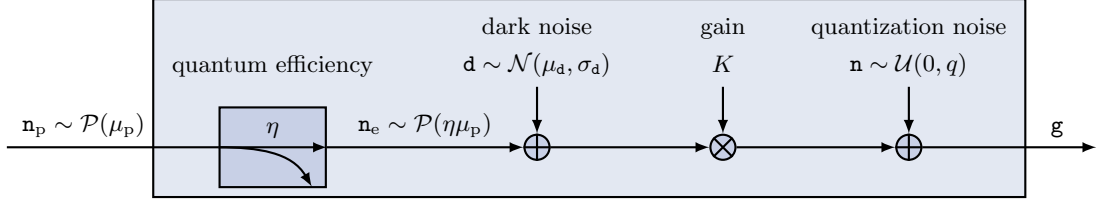
Figure 2: Schematic overview of the linear digital camera model according to the EMVA 1288 standard.

3. EMVA 1288 CAMERA MODEL

To objectively evaluate the proposed complementary sampling, a quantitative evaluation measure is needed. To this end, we employ the EMVA 1288 standard.[18] The standard introduces a digital camera model, calibration, and quantitative measures such as the camera's SNR to enable an objective comparison of different digital cameras. As of version 4 of the EMVA 1288 standard,[19] working with black-box cameras is supported. However, throughout this presentation we will employ the linear camera model as depicted in Figure 2. Here, $\mathbf{n}_\mathrm{p}$ denotes the incoming number of photons, which is usually assumed to Poisson-distributed with mean μ_p. Each incoming photon is absorbed by the sensor with a chance of η, called the quantum efficiency, resulting in $\mathbf{n}_\mathrm{e}$ electrons. This can be modelled as a Bernoulli experiment. The composition of the resulting Binomial distribution with a Poisson distribution yields again a Poisson distribution. This is also referred to as *thinning* of a Poisson distribution. The mean number of electrons is hence also Poisson-distributed with mean $\eta\mu_\mathrm{p}$. All of the sensor's sources of noise are incorporated into the dark noise $\mathbf{d}$ which is assumed to be normally distributed since it is the sum of multiple statistically independent (possibly unknown) noise sources. Usually, the largest contribution to the dark noise is the thermal noise which can be explicitly modelled. The electrons are read out and converted into a voltage which is amplified by the system gain K and digitized. The quantization is introduced using the linear quantization model by addition of the quantization noise $\mathbf{n}$ which is uniformly distributed. The output of the model is the digital greyscale value $\mathbf{g}$.

According to the EMVA 1288 standard, the wavelength dependence is only explicitly taken into account by the quantum efficiency. Furthermore, spectral effects are assumed to be linearly superimposed. That is, the incoming number of photons can be viewed as a collection of finitely many Poisson-distributed $\mathbf{n}_{\mathrm{p},i}$ with central wavelengths λ_i. Hence, the quantum efficiency is actually only sampled at these discrete central wavelenghts λ_i. Incorporating a spectral filter into this model is straightforward since the action of a spectral filter is essentially identical to that of the quantum efficiency $\eta(\lambda_i)$. That is, the filter's transmission coefficient $\varphi(\lambda_i)$ is interpreted as the probability of transmittance. Therefore, applying a spectral filter leads to a thinning of the Poisson distribution just as did the quantum efficiency. Now this thinned Poisson distribution can be viewed as the input to the camera model which leads to a mean number of electrons $\mu_\mathrm{e} = \eta(\lambda_i)\varphi(\lambda_i)\mu_{\mathrm{p},i}$. One can now interpret $\eta(\lambda_i)\varphi(\lambda_i)$ as an effective quantum efficiency of the camera and transfer all formulas and metrics specified by the EMVA 1288 standard by replacing

$$\eta(\lambda_i) \to \eta(\lambda_i)\varphi(\lambda_i)\,. \tag{18}$$

3.1 Signal-to-noise ratio

Using the linear camera model, one finds the mean and variance of the stochastic greyscale value

$$\mu_\mathbf{g} = \mu_\mathrm{d} + \eta\mu_\mathrm{p}\,, \tag{19}$$

$$\sigma_\mathbf{g}^2 = \sigma_0^2 + \eta\mu_\mathrm{p}\,, \tag{20}$$

where we have defined $\sigma_0^2 = \sigma_\mathrm{d}^2 + \sigma_\mathrm{q}^2/K$ for brevity. As one of the main values to compare digital cameras, the EMVA 1288 standard defines the (monochromatic)

$$\mathrm{SNR} = \frac{\mu_\mathbf{g} - \mu_\mathrm{d}}{\sigma_\mathbf{g}} = \frac{\eta\mu_\mathrm{p}}{\sqrt{\sigma_0^2 + \eta\mu_\mathrm{p}}}\,. \tag{21}$$

Here, a single calibrated monochromatic light source with a central wavelength close to the maximum of the camera's quantum efficiency is used to measure the required quantities. In that sense, the SNR defined above represents the highest possible SNR that can be achieved with the camera under consideration. The SNR of an ideal camera can easily be derived by neglecting the dark and quantization noise terms and using an ideal quantum efficiency $\eta = 1$, leading to

$$\text{SNR}_{\text{ideal}} = \sqrt{\mu_{\text{p}}}\,. \tag{22}$$

Note that even for an ideal camera, the photon noise still leads to a non-zero noise variance and thus yields an upper bound for the SNR.

The EMVA 1288 standard also specifies how to measure the SNR for color and spectral cameras: Given a camera with N color or spectral channels, one uses N monochromatic light sources with central wavelengths corresponding to the maxima of the N color filters φ_i. One than applies (21) to the quantities obtained from all monochromatic light source measurements independently, obtaining

$$\text{SNR}_i = \frac{\varphi_i(\lambda_i)\eta(\lambda_i)\mu_{\text{p},i}}{\sqrt{\sigma_0^2 + \varphi_i(\lambda_i)\eta(\lambda_i)\mu_{\text{p},i}}}\,, \quad i = 1, \ldots, N\,. \tag{23}$$

However, this procedure is limited to bandpass filters since it is ambiguous to refer to the filter's maxima in other instances. This in particular yields a problem when evaluating the proposed notch filter-based multispectral cameras. However, the problem also arises for other filter types such as highpass or lowpass filters which may also be suitable for multispectral imaging. Furthermore, measuring only with one light source per filter neglects effects depending on the filter width and filter overlap. This becomes quite clear in the case of the proposed notch filter imaging: Using a white light as input, the proposed technique yields a much higher power throughput than bandpass-based cameras as we have elaborated in Section 2. Furhtermore, large parts of the spectrum are sampled multiple times by different filters. However these characteristics are in no way reflected by the current EMVA 1288 standard.

3.2 Proposed extension

To overcome these limitations of the EMVA 1288 standard, we propose the following extension. For a spectral cameras with N spectral channels, i.e. using N different spectral filters φ_i of arbitrary type, one uses N monochromatic light sources with central wavelengths spread out equidistantly over the spectral range of interest. For example, when using bandpass filters these central wavelengths can be chosen to coincide with the central wavelengths of the used filters. In the case of the proposed notch-filters, the central lengths of the light sources are chosen to coincide with the absorption wavelength of the filters.

For every filter i one then measures the grey value $\mathbf{g}_{ij}$ *for all* light sources j obtaining

$$\mu_{\mathbf{g}_{ij}} = \mu_{\text{d}} + \varphi_i(\lambda_j)\eta(\lambda_j)\mu_{\text{p},j}\,, \tag{24}$$

$$\sigma_{\mathbf{g}_{ij}}^2 = \sigma_0^2 + \varphi_i(\lambda_j)\eta(\lambda_j)\mu_{\text{p},j}\,. \tag{25}$$

Accordingly, we generalize (23) to

$$\text{SNR}_{ij} = \frac{\varphi_i(\lambda_j)\eta(\lambda_j)\mu_{\text{p},j}}{\sqrt{\sigma_{\text{d}}^2 + \sigma_{\text{q}}^2/K + \varphi_i(\lambda_j)\eta(\lambda_j)\mu_{\text{p},j}}}\,, \quad i,j = 1, \ldots, N\,. \tag{26}$$

This way, the width and overlap of the spectral filters is explicitly taken into account and the individual SNR values provide inside into the camera's performance at different wavelengths for each channel. While the proposed extension increases the number of necessary measurements per camera by a factor of N, we believe it is the only meaningful backwards-compatible choice.

To reduce the above SNR definition to a single comparable quantity, we define the mean SNR to be the SNR of the random variable

$$\bar{\mathbf{g}} = \sum_{ij} \left(\mathbf{g}_{ij} - \mu_{\text{d}}\right)\,. \tag{27}$$

In the case of the conventional filters, we find the mean

$$\mu_{\bar{\mathbf{g}}} = \sum_{ij} \left(\mu_{\mathbf{g}_{ij}} - \mu_{\mathrm{d}} \right) = \sum_{ij} \varphi_i(\lambda_j)\eta(\lambda_j)\mu_{\mathrm{p},j} = \sum_j \eta(\lambda_j)\mu_{\mathrm{p},j} = \bar{\mu}_{\mathrm{p}} \tag{28}$$

where we have used the sum-to-one constraint (12) and defined $\bar{\mu}_{\mathrm{p}}$ as the mean total number of photons collected from all light sources as the stochastic analogue to the power P previously defined in (6). Analogously, we calculate the variance

$$\sigma_{\bar{\mathbf{g}}}^2 = \sum_{ij} \sigma_{\mathbf{g}_{ij}}^2 = \sum_{ij} \left(\sigma_0^2 + \varphi_i(\lambda_j)\eta(\lambda_j)\mu_{\mathrm{p},j} \right) = N^2\sigma_0^2 + \bar{\mu}_{\mathrm{p}} \tag{29}$$

and obtain the overall

$$\overline{\mathrm{SNR}} = \frac{\bar{\mu}_{\mathrm{p}}}{\sqrt{N^2\sigma_0^2 + \bar{\mu}_{\mathrm{p}}}} \tag{30}$$

which is conceptually very similar to the original definition (21). In a sense this can be viewed as the SNR obtained when capturing a white scene with the multispectral camera. In complete analogy to the ideal SNR of a monochromatic camera, we can calculate the ideal SNR by using $\varphi_i = 1 = \eta$ and $\sigma_0 = 0$ to obtain

$$\mathrm{SNR}_{\mathrm{ideal}} = \sqrt{N \sum_i \mu_{\mathrm{p},i}} \,. \tag{31}$$

In the case of the proposed complementary filters, we find the mean

$$\hat{\mu}_{\bar{\mathbf{g}}} = \sum_{ij} \left(\hat{\mu}_{\mathbf{g}_{ij}} - \mu_{\mathrm{d}} \right) = \sum_{ij} \hat{\varphi}_i(\lambda_j)\eta(\lambda_j)\mu_{\mathrm{p},j} = (N-1)\bar{\mu}_{\mathrm{p}} \tag{32}$$

and the variance

$$\hat{\sigma}_{\bar{\mathbf{g}}}^2 = \sum_{ij} \hat{\sigma}_{\mathbf{g}_{ij}}^2 = \sum_{ij} \left(\sigma_0^2 + \hat{\varphi}_i(\lambda_j)\eta(\lambda_j)\mu_{\mathrm{p},j} \right) = N^2\sigma_0^2 + (N-1)\bar{\mu}_{\mathrm{p}} \,. \tag{33}$$

Here, the mean total number of photons detected using the complementary filters is a factor of $(N-1)$ larger than in the conventional case which is the stochastic analogue of (17). Therefore, we find the overall

$$\widehat{\mathrm{SNR}} = \frac{(N-1)\bar{\mu}_{\mathrm{p}}}{\sqrt{N^2\sigma_0^2 + (N-1)\bar{\mu}_{\mathrm{p}}}} \,. \tag{34}$$

Finally, we find that the overall SNR in the case of the proposed complementary measurements is a factor $\sqrt{N-1}$ to $(N-1)$ larger than the SNR of the corresponding conventional measurements, depending on the strength of the camera's noise: when $\sigma_0 = 0$, we find $\widehat{\mathrm{SNR}} = \sqrt{N-1} \cdot \overline{\mathrm{SNR}}$. On the other hand, if σ_0 is much larger than $\bar{\mu}_{\mathrm{p}}$ it dominates the denominator, resulting in approximately $\widehat{\mathrm{SNR}} = (N-1) \cdot \overline{\mathrm{SNR}}$. We investigate this SNR in more detail in Section 4.

3.3 Basis transform

Using the noise model as specified by the EMVA 1288 standard, we investigate the SNR when performing the basis transform $\hat{\mathbf{x}} \to \mathbf{x}$. That is, given the complementary measurements $\hat{\mathbf{x}}$, how does the SNR behave when calculating the conventional spectral measurement $\mathbf{x}$ from it? As the stochastic analogue to the previously defined channel-wise measurements c_i, we define

$$\mathbf{c}_i = \sum_j \mathbf{g}_{ij} \tag{35}$$

with mean and variance

$$\mu_{\mathbf{c}_i} = N\mu_{\mathrm{d}} + \sum_j \varphi_i(\lambda_j)\eta(\lambda_j)\mu_{\mathrm{p},j} \,, \tag{36}$$

$$\sigma_{\mathbf{c}_i}^2 = N\sigma_0^2 + \sum_j \varphi_i(\lambda_j)\eta(\lambda_j)\mu_{\mathrm{p},j} \tag{37}$$

and analogously the complementary measurements $\hat{c}_i$ using the filters $\hat{\varphi}_i$. Note that, unlike previously, c_i does not correspond to a single measurement but to N measurements using the N different monochromatic light sources. When investigating the behaviour in the case of a single measurement and a given spectral flux, the noise terms would only appear once. Hence, the performance in the case of a single measurement will be better compared to the following.

First, we consider the case when a separate measurement of the power P is performed. That is, we perform additional measurements without any filters to calculate P and obtain the mean and variance

$$\mu_P = N\mu_d + \sum_j \eta(\lambda_j)\mu_{p,j}\,, \tag{38}$$

$$\sigma_P^2 = N\sigma_0^2 + \sum_j \eta(\lambda_j)\mu_{p,j}\,. \tag{39}$$

Then, we calculate the channel-wise transformation

$$\tilde{c}_i = P - \hat{c}_i \tag{40}$$

with mean

$$\mu_{\tilde{c}_i} = \mu_P - \mu_{\hat{c}_i} = \sum_j \eta(\lambda_j)\mu_{p,j} - \sum_j \hat{\varphi}_i(\lambda_j)\eta(\lambda_j)\mu_{p,j} = \sum_j \varphi_i(\lambda_j)\eta(\lambda_j)\mu_{p,j} \tag{41}$$

and variance

$$\sigma_{\tilde{c}_i}^2 = \sigma_P^2 + \sigma_{\hat{c}_i}^2 = 2N\sigma_0^2 + \sum_j \eta(\lambda_j)\mu_{p,j} + \sum_j \hat{\varphi}_i(\lambda_j)\eta(\lambda_j)\mu_{p,j} = 2N\sigma_0^2 + \bar{\mu}_p + \sum_j \hat{\varphi}_i(\lambda_j)\eta(\lambda_j)\mu_{p,j}\,. \tag{42}$$

We have used that the variables $\hat{c}_i$ and P are statistically independent and hence their covariance is zero. Since the mean of the dark current is in fact suppressed by the combination of the two measurements, we calculate the overall SNR as

$$\widehat{SNR} = \frac{\sum_i \mu_{\tilde{c}_i}}{\sqrt{\sum_i \sigma_{\tilde{c}_i}^2}} = \frac{\sum_{ij} \varphi_i(\lambda_j)\eta(\lambda_j)\mu_{p,j}}{\sqrt{\sum_i \left(2N\sigma_0^2 + \bar{\mu}_p + \sum_j \hat{\varphi}_i(\lambda_j)\eta(\lambda_j)\mu_{p,j}\right)}}$$
$$= \frac{\bar{\mu}_p}{\sqrt{2N^2\sigma_0^2 + N\bar{\mu}_p + (N-1)\bar{\mu}_p}} = \frac{\bar{\mu}_p}{\sqrt{2N^2\sigma_0^2 + (2N-1)\bar{\mu}_p}} \tag{43}$$

which is not as large as the original complementary measurement's $\widehat{SNR}$ (34) and even strictly smaller than the conventional $\overline{SNR}$ (30).

Now, when we calculate the power P from the complementary measurements directly, we perform the transform (16)

$$\tilde{c}_i = \frac{\sum_j \hat{c}_j}{N-1} - \hat{c}_i\,. \tag{44}$$

In a similar fashion to the above, we calculate the mean

$$\mu_{\tilde{c}_i} = \frac{\sum_j \mu_{\hat{c}_j}}{N-1} - \mu_{\hat{c}_i} = \frac{N}{N-1}\mu_d + \bar{\mu}_p - \sum_j \hat{\varphi}_i(\lambda_j)\eta(\lambda_j)\mu_{p,j} \tag{45}$$

and variance

$$\sigma_{\tilde{c}_i}^2 = \frac{\sum_j \sigma_{\hat{c}_j}^2}{(N-1)^2} + \sigma_{\hat{c}_i}^2 = \left[\left(\frac{N}{N-1}\right)^2 + N\right]\sigma_0^2 + \frac{1}{N-1}\bar{\mu}_p + \sum_j \hat{\varphi}_i(\lambda_j)\eta(\lambda_j)\mu_{p,j} \tag{46}$$

from which we find

$$\widetilde{\mathrm{SNR}} = \frac{\sum_i \left(\mu_{\tilde{c}_i} - \mu_d\right) - \mu_d}{\sqrt{\sum_i \sigma_{\tilde{c}_i}^2}} = \frac{\bar{\mu}_p + \frac{1}{N-1}\mu_d}{\sqrt{N\left[\left(\frac{N}{N-1}\right)^2 + N\right]\sigma_0^2 + \left(N + \frac{1}{N-1}\right)\bar{\mu}_p}} \approx \frac{\bar{\mu}_p}{\sqrt{N^2\sigma_0^2 + N\bar{\mu}_p}}, \qquad (47)$$

where the approximation holds for $N \gg 1$. Note, that in (43) and (47) the mean and the variance of the dark noise are the same for each measurement $\mathbf{g}_{ij}$. Thus it is assumed that the same exposure time is used for measurements without any filter, with bandpass filters and with complementary filters. We will investigate in detail the gain in SNR of the transformed variables compared to the conventional measurements in Section 4.

4. EXPERIMENTS

For the verification of the proposed approach we simulate the image formation process according to (4) and (9). To this end, we discretize the spectral domain by sampling the range $300\,\mathrm{nm} - 1100\,\mathrm{nm}$ in steps of $0.1\,\mathrm{nm}$. Throughout all simulations, the wavelength range of interest is the (extended) visible range, i.e. $\Lambda = [400\,\mathrm{nm}, 800\,\mathrm{nm}]$. The filters are spread out equidistantly across Λ as described in Section 2. For simplicity, we neglect the quantum efficiency $\eta(\lambda)$ in the simulations. However, if in a specific application the quantum efficiency is known, it is trivial to incorporate.

4.1 Sum-to-one constraint

As we have seen, in order for the complementary filter basis to be equivalent to the conventional one, one either has to measure the incoming power P separately (i.e. perform a measurement without any filter). Or, the filters need, at least approximately, satisfy the sum-to-one constraint (12). While the ideal rectangular bandpass naturally fulfil this constraint, this might not be true for other types, such as Gaussian bandpass and notch filters.

In the case of Gaussian notch filters, the constraint is visualized for different FWHMs of the complementary bandpass filters and different number of spectral channels in Figure 3. As expected, the constraint is not exactly fulfilled across the spectral range of interest. Furthermore, the deviation from the exact constraint also depends on the number of spectral channels and the FWHM of the filters. To investigate this in more detail, Figure 4 shows the average $\mathbb{E}_\lambda[\sigma(\lambda)]$ of the constraint across the spectral domain Λ for different numbers of spectral channels. It can be observed that for all considered FWHMs the constraint is on average fulfilled for some number of spectral channels. Hence, when designing the camera with a specific number of spectral channels, one can determine the optimal width of the notch filters by choosing the one with an average $\mathbb{E}_\lambda[\sigma(\lambda)] = 1$. In the case of the considered Gaussian notch filters, the solution can only be obtained numerically. The optimal FWHM is depicted in Figure 5. As expected, for a lower number of spectral channels, filters with a larger FWHM are ideal, while for higher number of spectral channels the ideal FWHM decreases. Comparing this curve with the width of the rectangular filters FWHM $= b = \Lambda/N$, the optimal FWHM is also inversely proportional to the number of filters N. Therefore, in the following we use $\mathrm{FWHM}_{\mathrm{opt}} = \Lambda/N$ also for the Gaussian filters. Note, that in the simulation the filters are assumed to have a maximum transmittance of exactly 1. Therefore, in a specific application using realistic filter shapes and values, the numeric optimization needs to be reevaluated.

4.2 SNR evaluation

To further evaluate the SNR of the proposed complementary spectral imaging, we apply the extended SNR definition (26) to a camera with Gaussian notch filters. As previously mentioned, the quantum efficiency $\eta(\lambda)$ is assumed to be constant. Therefore, the SNR is identical for all spectral channels and the shown average SNR. For the simulation of the measurements following the EMVA 1288 standard, we employ Gaussian-like light sources with central wavelengths identical to those of the used filters, following (1). The light sources are simulated with a FWHM $= 10\,\mathrm{nm}$. To illustrate the influence of the camera noise, we simulate two arbitrarily chosen values of the overall noise term $\sigma_0^2 = \sigma_d^2 + \sigma_q^2/K$.

Figure 6 shows the average SNR in the case of 11 spectral channels. The width of the Gaussian filters was optimally chosen to be $37.9\,\mathrm{nm}$ in accordance to the results given in Figure 5. Again, it can be observed that by
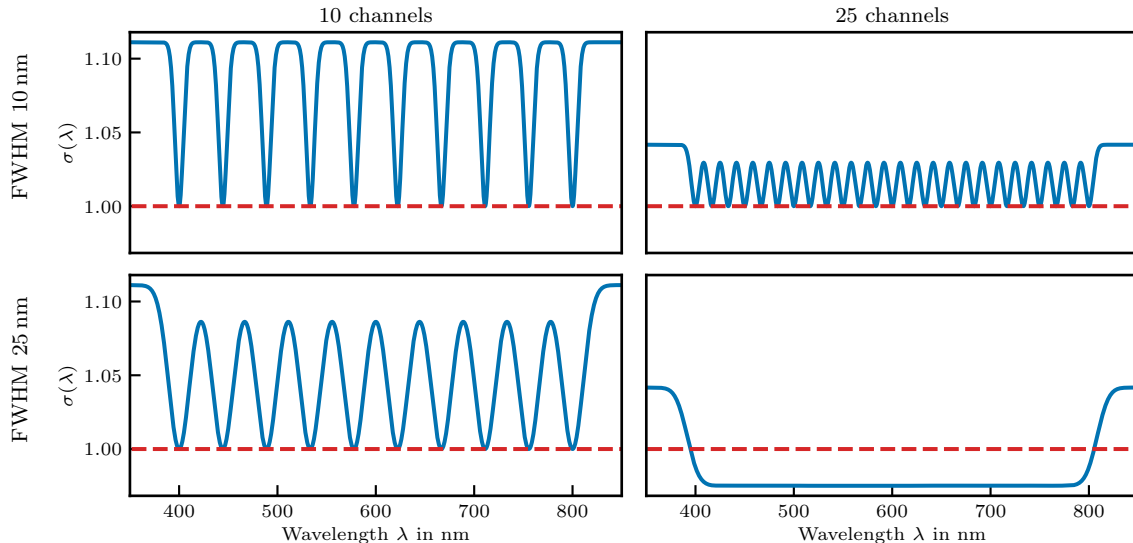
Figure 3: Sum-to-one constraint $\sigma(\lambda)$ for different number of channels and FWHM in the case of Gaussian notch filters.
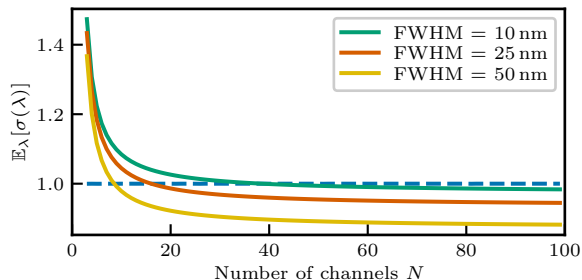

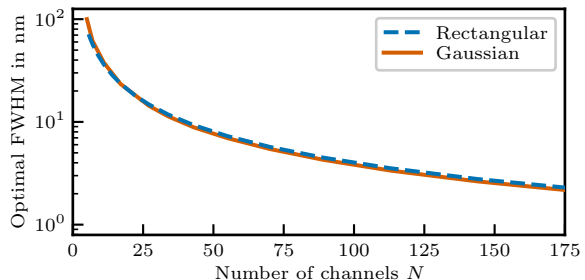Figure 4: Averaged sum-to-one constraint for Gaussian notch filters of different FWHMs.

Figure 5: Optimal FWHM with respect to the mean sum-to-one constraint for different number of spectral channels.

using complementary filters, the SNR is significantly improved compared to the SNR of conventional bandpass filters due to the larger amount of transmitted photons. For a large number of photons μ_p the variance σ_0^2 can be neglected and the SNR using the complementary filters is about a factor of $\sqrt{N-1} = 3.16$ larger than SNR using the conventional bandpass filters. For a small number of photons $\mu_{\mathrm{p},j}$ the effect of the noise is predominant which makes the improvement achieved by the complementary filters even more significant. The SNR for complementary filters at this point is $N - 1 = 10$ times larger than the SNR for bandpass filters. Note that the varying number of photons in this case is caused by a varying photon flux from the light source. The exposure time and thus the dark noise are constant in these calculations. In practise however this would not be the case. Given a scene with a fixed spectral flux, the exposure time in the case of the proposed complementary sampling approach would have to be much smaller than in the conventional case to yield the same digital greyscale value whilst avoiding overexposure. Therefore, the dark noise, which is approximately proportional to the exposure time due to the thermal noise, is much smaller in the proposed approach. In particular, this makes high resolution multispectral imaging much more feasible than with bandpass filters which often require special low noise cameras such as EM-CCD cameras which have to be heavily cooled down to reduce thermal noise. The comparison incorporating the exposure time and model of the dark noise is left for future research.

Varying the number of used spectral channels, it can be observed from Figure 7 that the SNR actually increases when using the complementary filters, as is expected. The more filters are used, the narrower the individual filters are due to the sum-to-one constraint. In the case of conventional bandpass filters, increasing the number of spectral channels results in a decreasing number of photons transmitting each filter. In the case of complementary filters however, an increased number of channels actually results in an increased number of photons transmitted by each filter. Using complementary filters, a high SNR can be achieved, especially at high spectral resolution.
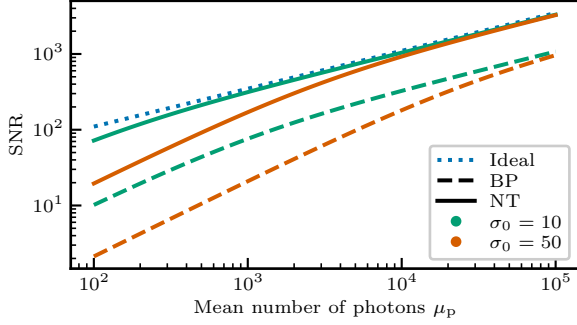
Figure 6: Mean SNR for Gaussian bandpass (BP) and complementary notch (NT) filters in the case of 11 spectral channels for different number of mean photons μ_p per light source.
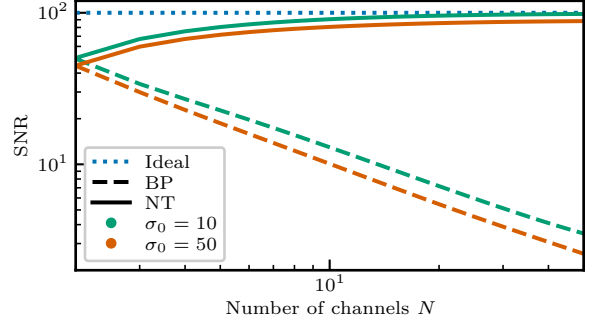

Figure 7: Mean SNR for a fixed number of mean photons $\mu_\mathrm{p} = 10^4$ for varying number of channels.
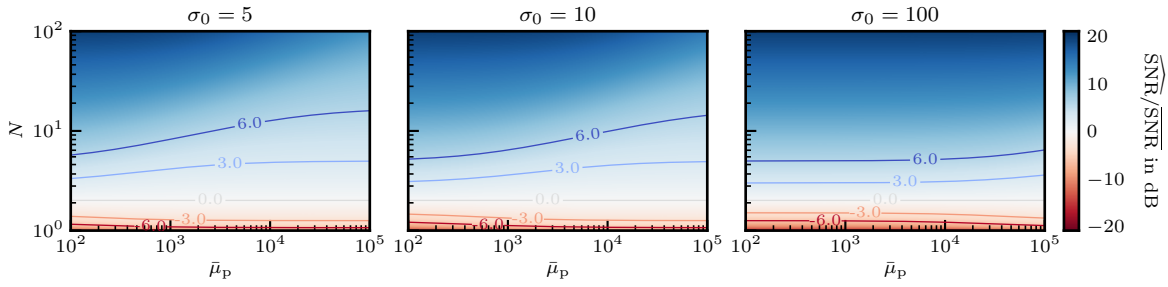

Figure 8: Ratio of the SNR of the complementary measurement and the conventional measurement according to (34) and (30). Blue indicates improvements over the conventional sampling approach.

In order to compare the sampling using bandpass filters and complementary filters more generally, the ratio $\widehat{\mathrm{SNR}}/\overline{\mathrm{SNR}}$ is examined according to (34) and (30) across all spectral channels. Figure 8 shows the ratio as a function of a varying number of photons $\bar{\mu}_\mathrm{p}$, a varying number of channels N as well as for different noise levels σ_0. For $N = 2$, $\widehat{\mathrm{SNR}}$ and $\overline{\mathrm{SNR}}$ are equal since in this case the bandpass and complementary filters are in fact equivalent. The SNR using complementary filters is larger than the SNR using bandpass filters for any constellation but especially for a large number of channels N. Even for a high noise level σ_0 or for a small number of photons $\bar{\mu}_\mathrm{p}$, corresponding to a small photon flux of the light sources, a much larger SNR is obtained using the proposed complementary sampling approach. In practical scenarios with 10 or more spectral channels, the SNR is about 6 dB larger in the proposed approach, further increasing with the numbers of spectral channels N.

Figures 9 and 10 show how the SNR using complementary filters behaves after a basis transformation compared to the original SNR using bandpass filters. Due to the transformation, the mean value μ_{c_i} of the signal decreases and is about the same as the mean value of the conventional signal using bandpass filters. The variance σ_P^2 of the signal, on the other hand, increases due to the increased number of measurements and is significantly larger than the variance of the conventionally sampled signal. If the power P is calculated from the complementary measurements directly, the number of measurements is increased by factor N compared to a direct measurement of P without any filters. Therefore, the variance of the dark noise and the photon noise is larger than the direct measurement's variance and the resulting SNR is smaller. If the basis transformation is performed using the power P, the resulting SNR is smaller than the SNR using bandpass filters for all considered cases. A direct transformation using $\hat{\mathsf{c}}_j$ improves the resulting SNR compared to a transformation via the power P, especially for a high noise levels σ_0, a small number of photons μ_{c_i} or a large number of channels N. For these parameters, the SNR after the basis transformation approaches the SNR using bandpass filters. Since the transformation can significantly degrade the SNR, we recommend evaluating the images in the complementary basis directly. The complementary image data is not a multispectral image in the conventional sense while containing the same spectral information.
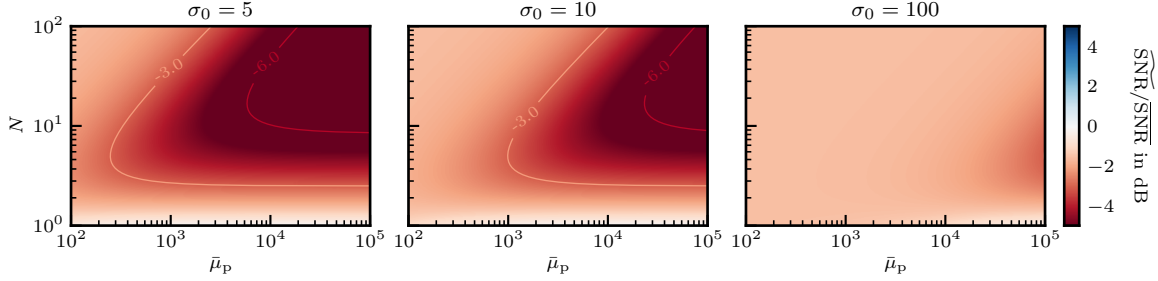
Figure 9: Ratio of the SNR of a conventional measurement obtained from the complementary measurement and an additional measurement of the power P and the directly measured conventional measurement according to (43) and (30).
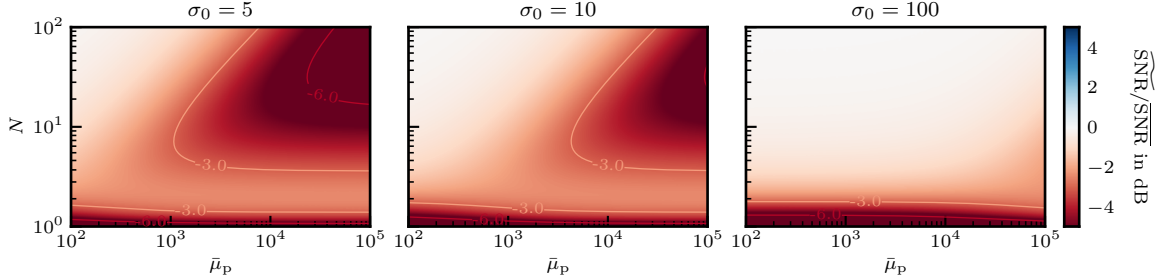

Figure 10: Ratio of the SNR of a conventional measurement obtained from the complementary measurement and the directly measured conventional measurement according to (47) and (30).

5. CONCLUSION

We proposed and evaluated a multispectral imaging approach using complementary notch filters to overcome the limitations present in bandpass filter-based multispectral imaging. By using complementary filters with transmission coefficients $\hat{\varphi}_i(\lambda) = 1 - \varphi_i(\lambda)$ instead of bandpass filters with transmission coefficients $\varphi_i(\lambda)$, the SNR of the multispectral measurements is improved significantly. This applies not only to ideal rectangular filters, but also to different types of filters, if the filters fulfil a sum-to-one constraint which we investigated in detail in the case of Gaussian filters.

Furthermore, we introduced an extension to the EMVA 1288 standard to overcome some of its limitations. In particular, the present standard is only applicable to bandpass filter-based color and multispectral cameras. We presented an extension, which contains the previous standard as a subset, to adapt the standard to arbitrary filter-based cameras. By illuminating all N channels with N monochromatic light sources, additional information about filter width and filter overlap is obtained. According to the presented detailed calculations and simulations, the resulting SNR using complementary filters is significantly higher than the SNR using bandpass filters, especially at high spectral resolution or in low-light environments. Therefore, it has great potential to increase the sensitivity of multispectral imaging- The complementary image data is not a multispectral image in the conventional sense while containing the same spectral information. A transformation of this data into the standard basis of bandpass filters is possible but the advantages of the complementary over the conventional approach, in terms of a higher SNR, are lost. Therefore, we recommend evaluating the data in the complementary basis, eliminating the need for further postprocessing. Hence, in the future we will investigate multispectral imaging applications, such as object classification, applied directly to the complementary image in comparison to the conventional measurements.

REFERENCES

[1] Borengasser, M., Hungate, W. S., and Watkins, R., [*Hyperspectral remote sensing: Principles and applications*], CRC Press (2007).

[2] Migdall, S., Klug, P., Denis, A., and Bach, H., "The additional value of hyperspectral data for smart farming," in [*2012 IEEE International Geoscience and Remote Sensing Symposium*], 7329–7332, IEEE (2012).

[3] Maddikunta, P. K. R., Hakak, S., Alazab, M., Bhattacharya, S., Gadekallu, T. R., Khan, W. Z., and Pham, Q.-V., "Unmanned aerial vehicles in smart agriculture: Applications, requirements, and challenges," *IEEE Sensors Journal* (2021).

[4] Krippner, W., Anastasiadis, J., and Puente León, F., "Robust iterative estimation of material abundances based on spectral filters exploiting the svd," in [*Algorithms, Technologies, and Applications for Multispectral and Hyperspectral Imagery XXV*], **10986**, 109861T, International Society for Optics and Photonics (2019).

[5] Lu, R. and Chen, Y.-R., "Hyperspectral imaging for safety inspection of food and agricultural products," in [*Pathogen Detection and Remediation for Safe Eating*], **3544**, 121–133, International Society for Optics and Photonics (1999).

[6] Tatzer, P., Wolf, M., and Panner, T., "Industrial application for inline material sorting using hyperspectral imaging in the NIR range," *Real-Time Imaging* **11**(2), 99–107 (2005).

[7] Lu, G. and Fei, B., "Medical hyperspectral imaging: A review," *Journal of Biomedical Optics* **19**(1), 010901 (2014).

[8] Qin, J., Chao, K., Kim, M. S., Lu, R., and Burks, T. F., "Hyperspectral and multispectral imaging for evaluating food safety and quality," *Journal of Food Engineering* **118**(2), 157–171 (2013).

[9] Gehm, M. E., John, R., Brady, D. J., Willett, R. M., and Schulz, T. J., "Single-shot compressive spectral imaging with a dual-disperser architecture," *Optics Express* **15**(21), 14013–14027 (2007).

[10] Wagadarikar, A., John, R., Willett, R., and Brady, D., "Single disperser design for coded aperture snapshot spectral imaging," *Applied Optics* **47**(10), B44–B51 (2008).

[11] Arce, G. R., Brady, D. J., Carin, L., Arguello, H., and Kittle, D. S., "Compressive coded aperture spectral imaging: An introduction," *IEEE Signal Processing Magazine* **31**(1), 105–115 (2013).

[12] Geelen, B., Tack, N., and Lambrechts, A., "A compact snapshot multispectral imager with a monolithically integrated per-pixel filter mosaic," in [*Advanced Fabrication Technologies for Micro/Nano Optics and Photonics VII*], **8974**, 89740L, International Society for Optics and Photonics (2014).

[13] Lambrechts, A., Gonzalez, P., Geelen, B., Soussan, P., Tack, K., and Jayapala, M., "A CMOS-compatible, integrated approach to hyper- and multispectral imaging," in [*2014 IEEE International Electron Devices Meeting*], 10.5.1–10.5.4 (2014).

[14] Parulski, K. A., "Color filters and processing alternatives for one-chip cameras," *IEEE Transactions on Electron Devices* **32**(8), 1381–1389 (1985).

[15] Baer, R. L., Holland, W. D., Holm, J. M., and Vora, P. L., "Comparison of primary and complementary color filters for CCD-based digital photography," in [*Sensors, Cameras, and Applications for Digital Photography*], **3650**, 16–25, International Society for Optics and Photonics (1999).

[16] Wang, X., Thomas, J.-B., Hardeberg, J. Y., and Gouton, P., "A study on the impact of spectral characteristics of filters on multispectral image acquisition," in [*12th Congress of the International Colour Association*], **4**, 1765–1768 (2013).

[17] Beyerer, J., León, F. P., and Frese, C., [*Machine vision – Automated visual inspection: Theory, practice and applications*], Springer (2015).

[18] European Machine Vision Association, "EMVA standard 1288 – Standard for characterization of image sensors and cameras." `www.emva.org` (2010).

[19] Jähne, B., "Release 4 of the EMVA 1288 standard: Adaption and extension to modern image sensors," in [*Forum Bildverarbeitung 2020*], 13, KIT Scientific Publishing (2020).